

# Autoregressive Generation of Static and Growing Trees

Hanxiao Wang  
CASIA, KAUST

Biao Zhang  
KAUST

Jonathan Klein  
KAUST

Dominik L. Michels  
KAUST

Dongming Yan  
CASIA

Peter Wonka  
KAUST

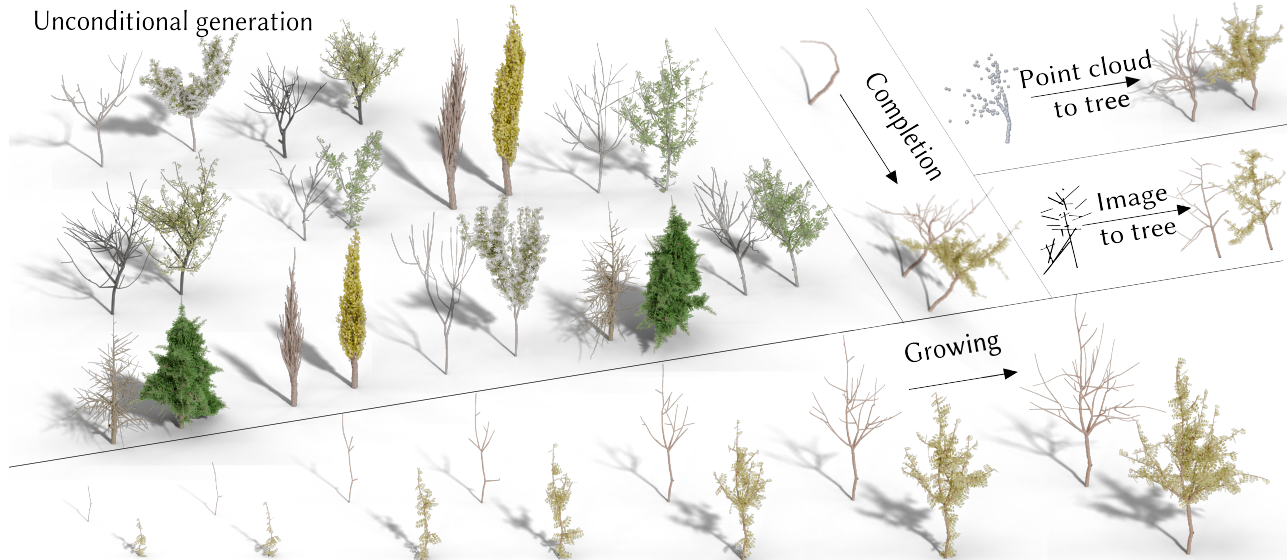


**Figure 1:** We introduce a data structure, transformer architecture, and training strategy for the autoregressive generation of trees. We show various applications such as the unconditional generation of static trees, the unconditional generation of growing trees, tree completion, point cloud to tree conversion, and 2D line sketch to tree conversion. Our method generates the tree skeleton while leaves are added procedurally.

## ABSTRACT

We propose a transformer architecture and training strategy for tree generation. The architecture processes data at multiple resolutions and has an hourglass shape, with middle layers processing fewer tokens than outer layers. Similar to convolutional networks, we introduce longer-range skip connections to complement this multi-resolution approach. The key advantages of this architecture are the faster processing speed and lower memory consumption. We are, therefore, able to process more complex trees than would be possible with a vanilla transformer architecture. Furthermore, we extend this approach to perform image-to-tree and point-cloud-to-tree conditional generation and to simulate the tree growth processes, generating 4D trees. Empirical results validate our approach in terms of speed, memory consumption, and generation quality.

## CCS CONCEPTS

• **Computing methodologies** → **Generative and developmental approaches**; *Shape analysis*; **Neural networks**.

## KEYWORDS

tree generation, hourglass transformer, growing trees, token ordering

## 1 INTRODUCTION

Tree generation is a classical problem in computer graphics and simulation. Trees typically exhibit complex hierarchical structures and diverse branching patterns. Traditional tree generation methods are mainly based on procedural techniques or rule-based simulations, which employ predefined growth rules or biological principles to produce plausible tree structures [De Reffye et al. 1988; Lewis 1999; Lindenmayer 1968; Reeves and Blau 1985; Smith 1984]. Although these approaches can be effective in specific settings, they require extensive parameter tuning and lack flexibility in adapting to different tree species and environments. Consequently, researchers continue to look for adaptive and scalable solutions capable of generating high-quality trees more efficiently.

The rise of deep generative models has opened up new avenues for generating complex structures. Notable examples include generative adversarial networks (GANs) [Goodfellow et al. 2020], variational autoencoders (VAEs) [Kingma 2013], autoregressive models [Esser et al. 2021], and diffusion models [Ho et al. 2020] which have demonstrated remarkable abilities in various modalities, such as images, text, point clouds, and videos [Chen et al. 2024c; Hao et al. 2024; Ho et al. 2022; Luo and Hu 2021; Vaswani 2017]. However, directly extending these deep generative methods to tree generation poses unique challenges. Trees possess hierarchical and recursive structures, in which branching patterns must maintain

spatial coherence while also following biological growth principles. Traditional deep generative methods, though highly effective for flat or non-recursive data, often face difficulties in maintaining structural consistency, preserving branch integrity, and achieving efficient training when applied to tree structures [Guo et al. 2020; Lee et al. 2025; Li et al. 2024; Zhou et al. 2023]. Therefore, a specialized approach remains necessary to fully harness the capabilities of deep generative models while respecting the core constraints of tree generation.

To tackle these challenges of tree generation, we propose a novel deep generative model that balances hierarchical structure preservation with computational efficiency. Our method introduces several key innovations that substantially improve the realism, coherence, and scalability of generated tree models.

- (1) The first deep generative approach explicitly tailored to tree structures. We present the first deep generative solution specifically designed for tree-structured data. By accounting for the hierarchical dependencies inherent in trees, our model provides greater flexibility and higher-quality tree generation compared to prior methods.
- (2) Streamlined parameterization and representation. We leverage an efficient parameterization strategy based on preorder traversal, which ensures hierarchical coherence while reducing parameter dimensionality. This design preserves structural integrity and improves computational efficiency, enabling faster training and inference even for large and complex trees.
- (3) Hourglass transformer for multi-resolution processing and improved training efficiency. We implement an *hourglass-shaped* transformer architecture [Hao et al. 2024; Nawrot et al. 2021], wherein the intermediate layers handle fewer tokens than the outer layers. We incorporate skip connections to complement the multi-resolution design. It yields faster processing speed and lower memory consumption, enabling us to handle more complex trees than conventional transformer architectures.
- (4) Extensions for conditional generation and 4D trees. Beyond unconditional generation, our framework supports image-to-tree and point-cloud-to-tree conditional generation and 4D tree growth simulations. The latter enables the dynamic evolution of trees while maintaining structural coherence. Empirical results confirm improvements in speed, memory usage, and overall generation quality across these tasks.

## 2 RELATED WORK

**Early tree modeling.** Early studies employed fractals and repetitive structures [Smith 1984], L-systems [Lindenmayer 1968; Prusinkiewicz 1986; Prusinkiewicz and Lindenmayer 2012], particle systems [Neubert et al. 2007; Reeves and Blau 1985], and biological growth rules [De Reffye et al. 1988]. The influence of physical and environmental conditions on the tree structure has also been taken into account, considering biomechanical properties [Maggioli et al. 2023; Wang et al. 2017; Zhao and Barbič 2013], fire [Pirk et al. 2017], wind [Pirk et al. 2014; Shao et al. 2021], and climate [Pałubicki et al. 2022]. The modeling of root systems has also been addressed for a variety of trees [Li et al. 2023]. On another trajectory, modeling large ecosystems [Makowski et al. 2019] has been addressed, as well as the simulation of devastating wildfires [Hädrich et al. 2021; Kokosza

et al. 2024] within these systems. A related problem is inverse procedural modeling, which aims to encode given inputs as a procedural model [Guo et al. 2020; Stava et al. 2014].

**Tree modeling using deep learning.** Advancements in deep learning have facilitated significant progress in tree generation, ranging from tree reconstruction from images [Li et al. 2021] to the use of transformer architectures to generate L-system grammars [Lee et al. 2023]. As relying on the syntax of the L-system restricts precise control over intricate details in generated structures, Zhou et al. [Zhou et al. 2023] explore deep learning for tree generation by focusing on the local context. However, their approach mainly considers the parent nodes and lacks comprehensive global structural awareness. Lee et al. [Lee et al. 2025] introduce a dataset and employ diffusion models to generate trees from a single image. Similarly, Li et al. [Li et al. 2024] utilize voxel-based diffusion to produce coarse semantic representations for tree reconstructions from single-view images.

These deep learning-based methods generally depend on indirect representations, such as L-systems or voxel-based diffusion techniques, which limit their ability to exert fine-grained control over tree structures. In contrast, our approach seeks to bridge this gap by investigating a native representation of trees, thereby facilitating more effective and detailed control over the generated models.

**3D generative modeling.** Generative models have made significant advancements, evolving from variational autoencoders (VAEs) [Kingma 2013] and generative adversarial networks (GANs) [Goodfellow et al. 2020] to diffusion models [Ho et al. 2020; Na et al. 2024; Song et al. 2020] and autoregressive models [Esser et al. 2021]. In 3D data generation, early approaches utilized voxel-based representations [Häne et al. 2017], which suffer from high memory consumption and limited resolution. Point cloud-based methods [Luo and Hu 2021] are more efficient but lack explicit surface connectivity. Implicit field-based models [Chen and Zhang 2019; Zhang et al. 2023; Zhang and Wonka 2024] represent 3D shapes as continuous functions, enabling high-resolution surface reconstruction but often requiring complex post-processing to extract meshes. Mesh-based generative models aim to generate 3D meshes with explicit surface representations directly [Alliegro et al. 2023; Chen et al. 2020].

Autoregressive transformer-based methods such as MeshGPT [Siddiqui et al. 2024], LLaMA-Mesh [Wang et al. 2024], MeshXL [Chen et al. 2024a], PivotMesh [Weng et al. 2024], and others have been proposed to improve mesh generation by predicting mesh elements using self-attention. MeshAnything [Chen et al. 2024b] and MeshAnythingV2 [Chen et al. 2024c], and EdgeRunner [Tang et al. 2024] implement mesh generation conditioned on point clouds. However, when performing unconditional generation, most of these methods can only generate meshes with 800 to 1600 faces, which is insufficient for modeling complex structures like trees. Our approach addresses this limitation by proposing a representation more suitable for tree modeling. Leveraging the properties of this representation, we propose to use an hourglass transformer architecture [Hao et al. 2024; Nawrot et al. 2021] to achieve higher efficiency and generate detailed meshes with significantly more faces, capturing the intricate structures of trees more effectively.

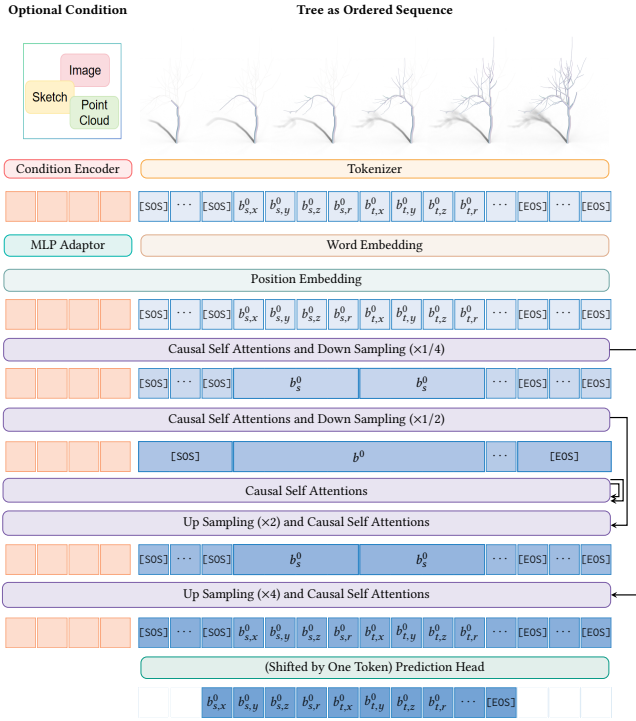


Figure 2: Architecture of our HourglassTree method

### 3 METHOD

This section presents our model, *HourglassTree*, which comprises a carefully designed tree representation and an Hourglass Transformer architecture. Section 3.1 introduces our tree representation and the tokenization method we employ. Section 3.2 details the Hourglass [Hao et al. 2024; Nawrot et al. 2021] Transformer architecture used for efficient learning.

#### 3.1 Tree Representation

**3.1.1 Parameterization.** Traditional methods for tree generation, including procedural and rule-based approaches, as well as growth simulations, often produce meshes with a very large number of faces, sometimes exceeding hundreds of thousands. This complexity poses challenges for face-based generation methods based on deep learning that typically handle meshes with considerably fewer faces.

To address this issue, we propose a more concise parameterization of trees by viewing a tree as a set of branches, which aligns closely with the natural characteristics of real-world trees. Each branch is represented as two end-points with associated radii, forming a cylinder in 3D space (see Fig. 3). Specifically, we define:

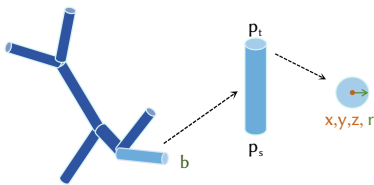


Figure 3: An illustration of our data structure.

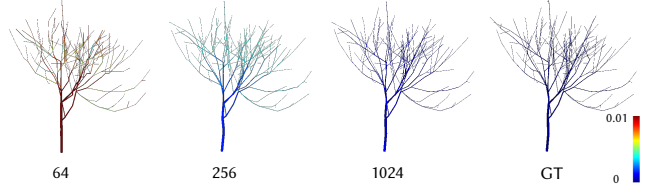


Figure 4: Different resolutions of data quantization.

- **Tree:**  $\tau = \{b^0, b^1, \dots, b^{n-1}\}$ , a set of  $n$  branches composing the entire tree structure. Note that  $\tau$  is an unordered set.
- **Branch:**  $b = (p_s, p_t)$  (or using the notation  $b^i = (b_s^i, b_t^i)$ ), a pair of vertices defining the branch’s two end-points.
- **Point:**  $p = (x, y, z, r)$ , where  $(x, y, z)$  denotes the 3D coordinates and  $r$  represents the radius at that vertex. We also use the notation  $b^i = ((b_{s,x}^i, b_{s,y}^i, b_{s,z}^i, b_{s,r}^i), (b_{t,x}^i, b_{t,y}^i, b_{t,z}^i, b_{t,r}^i))$ .

With this parameterization, a tree consisting of 200 branches requires only 1,600 parameters (each branch has 2 points, and each point has 4 parameters), significantly reducing the complexity compared to directly generating a mesh with over 100,000 parameters.

**3.1.2 Tokenization.** To utilize an autoregressive transformer model, we discretize the continuous parameters into discrete tokens. To balance complexity and quality, each continuous value is quantized into one of 256 bins (e.g. 256 distinct labels). The spatial coordinates  $(x, y, z)$  and the radius  $r$  use different bin boundary values due to their different statistical distributions, as shown in Fig. 4. We introduce special tokens for sequence control, including [SOS], [EOS], and [PAD] for sequence initialization, termination, and padding, respectively. For training efficiency, we prepend 8 [SOS] tokens and append 8 [EOS] tokens. For example, for elm trees, the sequence is padded to a fixed length of  $8 \times 202 = 1,616$  tokens, sufficient to represent a tree with 200 branches.

**3.1.3 Ordering of Branches.** The order of tokens is crucial for training autoregressive transformers. Some existing approaches sort mesh elements based on spatial coordinates or employ specifically designed ordering strategies. In our setting, we define an ordering for the branches that captures the structural dependencies inherent in tree geometry.

A popular approach is to sort branches by their zyx order (sorting by  $z$  then by  $y$  then by  $x$  coordinates descendingly) [Nash et al. 2020], as shown in Figure 5. This is also observed in the image context, where the simplest ordering tends to be the best [Esser et al. 2021]. In point cloud learning, OctFormer and PTv3 employ Hilbert ordering instead [Wang 2023; Wu et al. 2024].

However, these methods fail to capture causal, parent-child relationships between branches and can lead to disconnected or physically implausible structures.

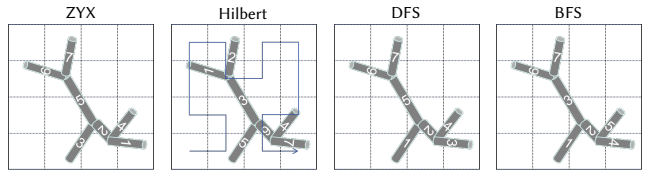


Figure 5: Different strategies for ordering tokens.

Surprisingly, we found significantly better ordering strategies in the context of the trees. We first construct a tree graph representing the (botanical) tree’s branching structure, where each node corresponds to a branch  $b_i$  and edges capture parent-child relationships. We then traverse the tree using depth-first search (DFS) or breadth-first search (BFS). These traversal strategies determine the order of branches in the token sequence, ensuring that the hierarchical relationships within the tree are properly encoded. With these algorithms, we obtain a flattened sequence  $\tau_\pi = \pi(\tau)$  where  $\pi(\cdot)$  represents a permutation applied to the original set.

This approach aligns with the tree’s inherent structure and facilitates more coherent generation results by preserving the dependencies among branches. Additionally, these traversal methods ensure that each branch can inherit information from its ancestor nodes, further enhancing the consistency of the generation process.

### 3.2 Hourglass Transformer Architecture

Given the structured token sequence, we adopt an Hourglass Transformer [Hao et al. 2024; Nawrot et al. 2021] architecture to efficiently model long-range dependencies and hierarchical structure inherent in tree data.

**3.2.1 Architecture Overview.** As shown in Fig. 2, the Hourglass Transformer employs a U-Net-like architecture, comprising distinct downsampling and upsampling stages interconnected via shift skip connections. This hierarchical design enables the model to effectively capture both global and local patterns within the input data, making it particularly suitable for tasks such as tree generation.

**3.2.2 Downsampling and Self-Attention.** Our network is specifically designed for structured trees with inherent structural. To aggregate this information progressively, the model utilizes a hierarchical downsampling strategy (local average pooling):

- **First Downsampling:** Reduces the sequence length by a factor of four (merging a quadruple of x, y, z, and r), resulting in each token representing one vertex of a branch.
- **Second Downsampling:** Further decreases the sequence length by a factor of two (merging two vertices), with each token corresponding to an entire branch.

At each downsampling scale, *only one* self-attention layer is applied to model dependencies among tokens. Note that this differs from other U-Net style transformers, which still apply several layers in the outer stages.

**3.2.3 Bottleneck.** The bottleneck component serves as an intermediary between the downsampling and upsampling stages. We build a mini-UNet-style bottleneck in the bottleneck which is proved to be effective in the experiments. The latter half of the bottleneck layers are connected to the first half, like a UNet. In addition to the skip connections, we assign scales (learned during network training) to the first half of the layers,

$$b^i \leftarrow b^i + \alpha \circ, \quad (1)$$

where  $\alpha$  is the learned scale parameter, and  $\circ$  represents the features from the first half of the layers.

This mechanism ensures that features captured in the earlier stages are adaptively reintroduced during the later stages, allowing

the model to effectively utilize information from both ends of the bottleneck for more refined transformations.

**3.2.4 Upsampling and Self-Attention.** In the decoder part, each compressed token is first upsampled (duplicated) to multiple ones. For example, the feature for branch  $b^i$  is duplicated to  $b_s^i$  and  $b_t^i$  which represent the features for the two end-points of the branch  $b^i$ . Similarly for  $b^j$  which is duplicated to  $(b_{s,x}^j, b_{s,y}^j, b_{s,z}^j, b_{s,r}^j)$ . We perform *only one* causal self-attention layer and connect it with the (shifted) outputs from the encoder side:

$$\begin{aligned} b_s^i &\leftarrow \text{CausalSA}(\text{Upsample}(b_s^i) + \text{Shift}(b_s^i, \text{Encoder})) \\ b_t^i &\leftarrow \text{CausalSA}(\text{Upsample}(b_t^i) + \text{Shift}(b_t^i, \text{Encoder})) \end{aligned} \quad (2)$$

$\text{Shift}(\cdot, \text{Encoder})$  represents the element in the Encoder’s output sequence shifted left by one. We perform a similar operation for the sequence  $((b_{s,x}^i, b_{s,y}^i, b_{s,z}^i, b_{s,r}^i), (b_{t,x}^i, b_{t,y}^i, b_{t,z}^i, b_{t,r}^i))$ .

**3.2.5 Training Objective.** We train the autoregressive transformer using the standard cross-entropy loss. Given a training dataset of tokenized trees, the loss function is as follows.

$$\mathcal{L} = - \sum_{j=1}^{8n} \log P(\square_j | \square_{<j}; \theta), \quad (3)$$

where  $8n$  is the total sequence length,  $\square_i$  is the  $i$ -th token in the sequence,  $\square_{<i}$  represents all the tokens before  $\square_i$ , and  $\theta$  denotes the model parameters.

**3.2.6 Inference.** During sampling, the sequence length must be a multiplier of 8. To handle input sequences that do not perfectly align with the downsampling factors, the model includes padding operations to adjust the sequence length to the nearest multiple required by the downsampling layers.

## 4 EXPERIMENTS

For all experiments, unless otherwise stated, we employ data augmentation techniques, including random rotation along the z-axis and mirroring. The total batch size is set to 64, and the model is optimized using the AdamW optimizer with a learning rate of  $5 \times 10^{-3}$ . A warm-up period of 5 epochs is followed by a CosineAnnealingLR learning rate decay schedule. Flash Attention 2 is utilized for the attention mechanism. The training is conducted on 4 NVIDIA A100 GPUs (80GB each).

All experiments utilized a transformer architecture with 24 layers. The first two downsampling layers each consist of one layer, followed by a bottleneck of 20 layers. The final two upsampling layers each comprised one layer. The transformer has 79,398,144 parameters, with an embedding dimension of 512 and 16 attention heads. For the Vision Transformer (ViT) encoder, we used the CLIP ViT from the timm library [Wightman 2019].

The training dataset was generated using the provided source code of the botanical tree growth model presented in [Li et al. 2023]. Their package also provides realistic growth parameters for various tree species (represented as a 70-dimensional vector for each species), from which we selected the 6 species used in this paper.

For elm trees, we processed the dataset to limit each tree to a maximum of 200 branches and trained the model for 20 epochs. For

other tree species, we limited each tree to up to 1,000 branches and trained for 30 epochs. In unconditional generation experiments, we utilized a dataset of 10,000 samples, divided into 9,000 for training and 1,000 for testing. In the conditional generation experiments, we employed 50,000 samples for training and 1,000 for testing, training for 50 epochs. In the Tree Growth Dynamics experiments, we generated sequences with a length of  $1027 \times 8$ , training for 50 epochs. on 19,118 samples and testing on 1,000 samples.

#### 4.1 Evaluation Metrics

To comprehensively assess the performance of our generative model, we employ a set of evaluation metrics that capture various aspects of the generated samples, including their novelty, uniqueness, quality, and similarity to real data distributions. The metrics are as follows:

- **FID (Fréchet Inception Distance):** Measures the distance between the generated and real data distribution; lower values indicate higher fidelity.
- **PPL (Perplexity):** Evaluates the stability and predictability of the generated sequences; lower values signify more coherent and stable generated results.
- **Connect:** Assesses the connectivity of the generated structures; higher values denote better structural coherence.
- **Novel:** Indicates the proportion of generated samples that are novel; a value of 1.0000 implies all samples are novel.
- **Unique:** Measures the uniqueness of generated samples; a value of 1.0000 implies all samples are unique.
- **MMD-CD (Maximum Mean Discrepancy - Chamfer Distance):** Quantifies the similarity between generated and real data distributions using Chamfer Distance; lower values indicate closer alignment.
- **COV-CD (Coverage - Chamfer Distance):** Measures the coverage of the real data distribution by the generated samples using Chamfer Distance; higher values denote better coverage.
- **JSD (Jensen-Shannon Divergence):** Evaluates the similarity between the generated and real data distributions; lower values indicate higher similarity.
- **IoU (Intersection over Union):** Measures the overlap between the generated image and the ground truth; higher values indicate better alignment.
- **Precision:** Assesses the accuracy of the generated structures in terms of correctly predicted elements; higher values indicate fewer false positives.
- **Recall:** Evaluates the ability of the model to capture all relevant elements of the real data; higher values indicate fewer false negatives.
- **F1-Score:** Combines Precision and Recall into a single metric by taking their harmonic mean; higher values indicate a better balance between Precision and Recall.

#### 4.2 Unconditional Generation

We present the results of unconditional generation experiments. We begin by exploring various token-ordering strategies. An ablation study is then conducted to evaluate the impact of specific design components on performance. Finally, we demonstrate the model’s capability to generate diverse species, as illustrated in Fig. 11.

**4.2.1 Token Ordering Strategies.** In our experiment on token ordering strategies, we evaluated four distinct methods—*zyx*, *Hilbert*, *DFS*, and *BFS* on *Elm* trees—across a comprehensive set of metrics, as presented in Table 1.

**Table 1: Performance of different token ordering strategies.**

Metric	<i>zyx</i>	<i>hilbert</i>	<i>dfs</i>	<i>bfs</i>
<b>FID Score</b> ↓	36.30	83.36	<b>5.64</b>	10.21
<b>Connect</b> ↑	0.6233	0.2290	<b>0.9866</b>	0.9466
<b>Novel</b> ↑	<b>1.0000</b>	<b>1.0000</b>	<b>1.0000</b>	<b>1.0000</b>
<b>Unique</b> ↑	<b>1.0000</b>	<b>1.0000</b>	<b>1.0000</b>	<b>1.0000</b>
<b>MMD-CD</b> ↓	0.0291	0.0260	<b>0.0242</b>	0.0268
<b>COV-CD</b> ↑	0.4440	0.3850	<b>0.5180</b>	0.4850
<b>JSD</b> ↓	0.0607	0.1012	0.0406	<b>0.0375</b>

The results demonstrate that the *DFS* token ordering strategy achieves the best performance. It attains the lowest FID and the highest connectivity, reflecting its strong generative quality and structural coherence. Furthermore, *DFS* maintains perfect novelty and uniqueness, indicating that its generated samples remain both distinct and diverse. The *BFS* strategy also performs well, with an FID of 10.21, connectivity of 0.9466, and similarly favorable coverage and MMD-CD metrics.

In contrast, both *zyx* and *Hilbert* exhibit substantially higher FID scores, suggesting lower generative quality. Their connectivity values (0.6233 and 0.2290, respectively) are also less favorable, although they retain perfect novelty and uniqueness. These findings confirm that while all ordering methods produce new and unique structures, the ability to capture the underlying data distribution and preserve coherent connections strongly depends on the chosen ordering strategy, as shown in Fig. 6.



**Figure 6: Tree structures generated using different token orders.**

These results emphasize the critical impact of token ordering on generative performance. With *DFS* and *BFS* outperforming *zyx* and *Hilbert* across multiple evaluation metrics, we see clear evidence that a carefully designed token ordering strategy is essential for high-quality and diverse tree generation.

**4.2.2 Ablation Study.** To dissect the contributions of specific design components, an ablation study was conducted comparing five different model variants, as detailed in Table 2. The variants include: **PT (Plain Transformer)** as the baseline architecture, **HG1 (Hourglass 1)** incorporating an hourglass structure with one down-sampling layer, **HG2 (Hourglass 2)** incorporating an hourglass structure with two down-sampling layers, **HG2+R (Hourglass 2 with Bottleneck Residual)**, which adds non-learnable bottleneck residuals to HG2, and **HG2+R+L (Hourglass 2 with Learnable Bottleneck Residual)** (or **Full**), which enhances HG2 with learnable bottleneck residuals.

**Table 2: Performance comparison of different models. The best results in each metric are highlighted in bold.**

Metric	PT	HG1	HG2	+R	+L (Full)
FID ↓	9.111	9.263	6.186	5.996	<b>5.641</b>
Time	10m 15s	<b>5m 13s</b>	5m 20s	5m 21s	5m 21s
GPU	15.9G × 4	<b>5.5G × 4</b>	6.0G × 4	6.1G × 4	6.1G × 4

The baseline **PT** exhibited a high FID of 9.111, the longest training time of 10 minutes and 15 seconds, and the highest GPU memory usage at 15.9G × 4. Introducing a single down-sampling layer in **HG1** decreased the training time to 5 minutes and 13 seconds, while GPU memory usage dropped to 5.5G × 4, but yields a similar FID with **PT**. Adding a second down-sampling layer in **HG2** substantially improved the FID to 6.186 with minimal changes to training time and GPU memory consumption. The **HG2+R** variant, which incorporates non-learnable bottleneck residuals, achieved a reduction in FID to 5.996, with a slight increase in GPU usage to 6.1G × 4. Finally, the **Full** model, featuring learnable bottleneck residuals, attained the best FID of 5.641 while maintaining comparable training time and GPU memory usage to **HG2+R**.

**Table 3: Performance metrics of the model for different data sizes, showcasing scalability. Rows represent respective metrics with ↑ indicating higher is better and ↓ indicating lower is better.**

Metric	9k	25k	50k
FID Score ↓	5.6413	3.1792	<b>2.9701</b>
Connect ↑	0.9866	0.9983	<b>0.9994</b>
PPL ↓	0.8367	0.7847	<b>0.7717</b>

**4.2.3 Scalability.** Table 3 presents the evaluation metrics of the model for different dataset sizes: 9k, 25k, and 50k. These sizes correspond to varying amounts of training data, allowing us to assess the model’s scalability. The model shows strong scalability as the training data increases. The improvements in FID score, Connect, and PPL suggest that the model becomes more efficient and capable of generating high-quality, structurally sound, and diverse data as it is trained on larger datasets. These results emphasize the model’s potential for scaling to handle larger and more complex datasets effectively.

**4.2.4 Different species generation.** We present the results of our unconditional generation experiments. We trained 6 models for each species, including **Vitellaria**, **Hickory**, **Shadbush**, **Spruce**, and **Tulip**. As shown in Fig. 11, our model is capable of generating diverse species with high fidelity. The generated samples exhibit significant variations in structure and appearance, demonstrating the model’s capability to capture intricate patterns and characteristics inherent to different species.

Table 4 summarizes the performance metrics of different tree structures generated by our model. Each row represents a specific evaluation metric. Notably, the model demonstrates high-quality results, with diverse and unique samples across all species, as indicated by the Unique and Novel metrics being consistently at their maximum value of 1.0. Additionally, the FID scores, which assess the fidelity of the generated samples, are relatively low across species,

**Table 4: Performance metrics of different tree structures. Rows represent respective metrics with ↑ indicating higher is better and ↓ indicating lower is better.**

Metric	Vitellaria	Hickory	Shadbush	Spruce	Tulip
FID Score ↓	28.96	30.40	32.10	14.98	16.65
Connect ↑	0.9801	0.9880	0.9616	0.9825	0.9901
Novel ↑	1.0000	1.0000	1.0000	1.0000	1.0000
Unique ↑	1.0000	1.0000	1.0000	1.0000	1.0000
MMD-CD ↓	0.0390	0.0356	0.0247	0.0217	0.0048
COV-CD ↑	0.3060	0.3010	0.4420	0.3820	0.4300
JSD ↓	0.0959	0.1139	0.0976	0.0618	0.0378

further suggesting the model’s capability to generate high-fidelity tree structures. For the performance of the **Elm** species, please refer to Table 1.

### 4.3 Modeling and Generating Tree Growth Dynamics

In this section, we transform the ten distinct stages of tree growth into ten separate token lists, each representing a different development stage, and subsequently concatenate these lists in chronological order to form a single, continuous token sequence. As shown in Fig. 13, by employing an autoregressive generation approach, the model systematically learns and reconstructs the tree’s dynamic evolution from its initial sprout to full maturity. Concatenating the stage-wise token lists in this manner explicitly models the transitions between consecutive stages, thereby capturing critical inter-stage relationships that drive the tree’s morphological development over time. Moreover, the autoregressive framework leverages the entirety of the preceding stages to maintain and refine the details of the growth process. Consequently, the final generated sequence comprehensively depicts the tree’s complete growth trajectory.

### 4.4 Conditional Generation

**4.4.1 Completion.** Our model enables us to take a partial tree structure as an autoregressive prompt and continue generating the tree based on this initial input. As illustrated in Fig. 12, given an incomplete tree, our model can extend it into a diverse set of complete tree structures.

**Table 5: Comparison of DFS and BFS ordering.**

Metric	IoU ↑	Precision ↑	Recall ↑	F1-Score ↑
BFS	0.2657	0.4038	0.4295	0.4153
DFS	<b>0.3045</b>	<b>0.4332</b>	<b>0.4958</b>	<b>0.4615</b>

**4.4.2 Image to tree.** We explore the performance differences between Depth-First Search (DFS) and Breadth-First Search (BFS) strategies in the *image2trees* task. As illustrated in Table 5, DFS outperforms BFS across all evaluation metrics. Specifically, DFS achieves an Intersection over Union (IoU) of 0.3045, which is significantly higher than BFS’s 0.2657. Precision and Recall are improved by approximately 7% and 15%, respectively, while the F1-Score increases by about 11%. These results indicate that DFS is more effective in capturing key information from images when generating tree structures, thereby enhancing the overall quality of the generated results.

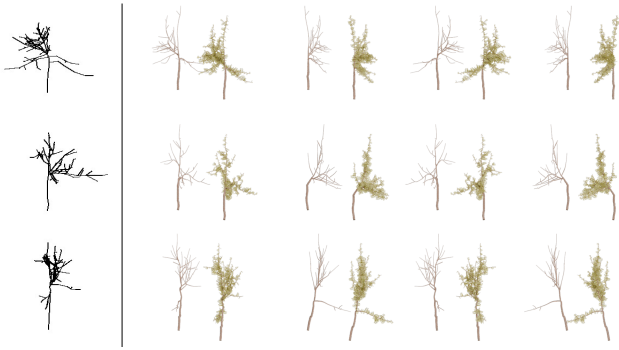


**Figure 7: Tree structures generated using DFS token order. The first column illustrates the input image, while the subsequent four columns display different views of the resulting tree structures.**

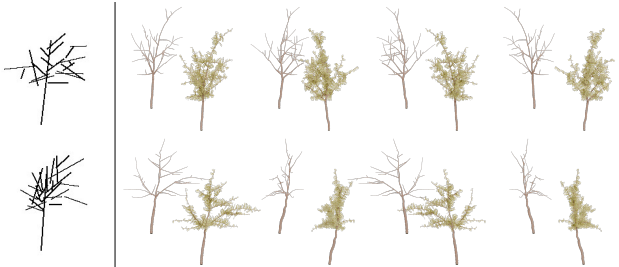


**Figure 8: Tree structures conditioned on 2D vector graphics.**

Fig. 9 presents examples of tree structures generated using DFS and BFS. The trees generated by DFS exhibit more detailed and accurate node distributions with a deeper hierarchical organization. In contrast, those generated by BFS tend to be more balanced but may fail to capture finer details. This further validates the effectiveness of DFS in this task. Fig. 7 shows different views of the resulting tree structures using DFS token order.

Using our framework for training, we can also generate reasonable trees conditioned on hand-drawn 2D vector graphics, as shown in Fig. 8. We successfully satisfy the intent of the interactive sketch in the main structure while generating diverse and plausible 3D branches, even though the input 2D vectors in the picture are not connected.

To achieve interactive tree modeling, we trained a conditional generative model using 2D vector graphics. Specifically, we projected the two endpoints of tree branches onto a 2D plane and rendered them as line segments, resulting in 2D vector graphics.

**4.4.3 Point cloud to tree.** To achieve the generation of tree structures from sparse point cloud data, we randomly sample 200 points for each tree as the condition. We employ an approach that leverages 50 learnable query vectors and point cloud embeddings within a cross-attention framework. This cross-attention mechanism effectively integrates the geometric information of the input point cloud into a fixed-length token list.

Once the point cloud information is infused into the token list, it is utilized as a prompt for our tree autoregressive generation model.



**Figure 9: Comparison of tree structures generated using DFS and BFS token order.**

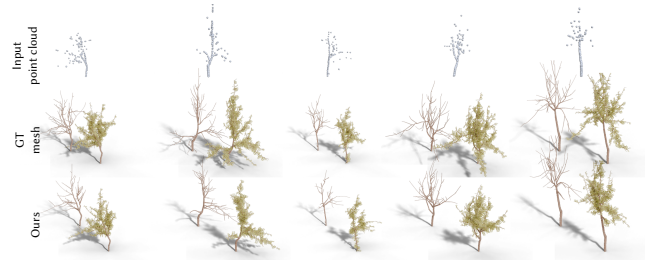


**Figure 10: Point cloud to tree examples.**

This model sequentially generates the tree structure, guided by the constraints and features extracted from the input point cloud. As depicted in Fig. 10, our experimental results demonstrate that the generated tree models adhere closely to the input point cloud constraints, ensuring the overall structure aligns with the provided geometric data.

## 5 CONCLUSION AND FUTURE WORK

We introduced *HourglassTree*, an innovative transformer-based architecture specifically engineered to generate 3D tree structures. We propose an efficient data structure, an hourglass-shaped transformer architecture, and suitable token ordering strategies for efficiently managing hierarchical tree data. Our framework extends to 4D growing trees and conditional generation tasks, including tree completion, image-to-tree, and point-cloud-to-tree generation.

Future work will explore several aspects to further enhance *HourglassTree*. First, we aim to expand the scope of our approach to encompass a broader range of applications beyond trees, such as generating other organic or hierarchical structures (e.g., vascular systems, urban layouts, or molecular assemblies). Additionally, we will focus on optimizing the architecture to handle increasingly complex and larger-scale tree structures, potentially incorporating hierarchical parallelism and advanced memory management techniques. Investigating the application of linear attention mechanisms in tree generation tasks also presents a promising direction for enhancing efficiency and scalability.

In conclusion, *HourglassTree* establishes a robust foundation for the next generation of deep generative tree models. We anticipate this work will inspire further research and development for generating structured 3D and 4D data.

## REFERENCES

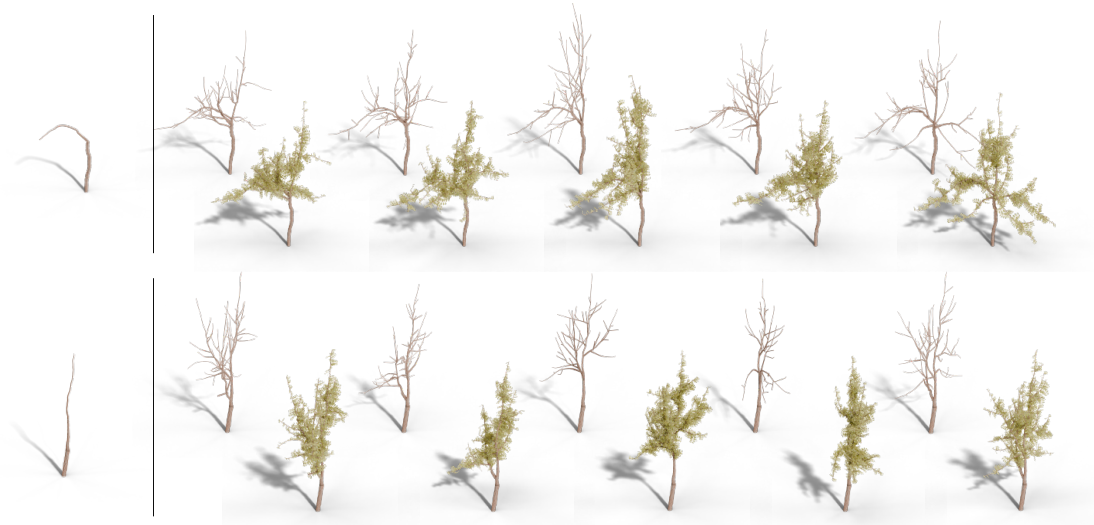
- A. Alliegro, Y. Siddiqui, T. Tommasi, and M. Nießner. 2023. Polydiff: Generating 3d polygonal meshes with diffusion models. *arXiv:2312.11417* (2023).
- S. Chen, X. Chen, A. Pang, X. Zeng, W. Cheng, Y. Fu, F. Yin, Y. Wang, Z. Wang, C. Zhang, et al. 2024a. MeshXL: Neural Coordinate Field for Generative 3D Foundation Models. *arXiv:2405.20853* (2024).
- Y. Chen, T. He, D. Huang, W. Ye, S. Chen, J. Tang, X. Chen, Z. Cai, L. Yang, G. Yu, et al. 2024b. MeshAnything: Artist-Created Mesh Generation with Autoregressive Transformers. *arXiv:2406.10163* (2024).
- Y. Chen, Y. Wang, Y. Luo, Z. Wang, Z. Chen, J. Zhu, C. Zhang, and G. Lin. 2024c. Meshanything v2: Artist-created mesh generation with adjacent mesh tokenization. *arXiv:2408.02555* (2024).
- Z. Chen, A. Tagliasacchi, and H. Zhang. 2020. Bsp-net: Generating compact meshes via binary space partitioning. In *Proceedings of the IEEE/CVF conference on computer vision and pattern recognition*. 45–54.
- Z. Chen and H. Zhang. 2019. Learning implicit fields for generative shape modeling. In *Proceedings of the IEEE/CVF conference on computer vision and pattern recognition*. 5939–5948.
- P. De Reffye, C. Edelin, J. Françon, M. Jaeger, and C. Puech. 1988. Plant models faithful to botanical structure and development. *ACM Siggraph Computer Graphics* 22, 4 (1988), 151–158.
- P. Esser, R. Rombach, and B. Ommer. 2021. Taming transformers for high-resolution image synthesis. In *Proceedings of the IEEE/CVF conference on computer vision and pattern recognition*. 12873–12883.
- I. Goodfellow, J. Pouget-Abadie, M. Mirza, B. Xu, D. Warde-Farley, S. Ozair, A. Courville, and Y. Bengio. 2020. Generative adversarial networks. *Commun. ACM* 63, 11 (Oct. 2020), 139–144. <https://doi.org/10.1145/3422622>
- J. Guo, H. Jiang, B. Benes, O. Deussen, X. Zhang, D. Lischinski, and H. Huang. 2020. Inverse procedural modeling of branching structures by inferring l-systems. *ACM Transactions on Graphics (TOG)* 39, 5 (2020), 1–13.
- T. Hädrich, D. T. Banuti, W. Palubicki, S. Pirk, and D. L. Michels. 2021. Fire in Paradise: Mesoscale Simulation of Wildfires. *ACM Transaction on Graphics* 40, 4, Article 163 (08 2021). <https://doi.org/10.1145/3450626.3459954>
- C. Häne, S. Tulsiani, and J. Malik. 2017. Hierarchical surface prediction for 3d object reconstruction. In *2017 International Conference on 3D Vision (3DV)*. IEEE, 412–420.
- Z. Hao, D. W. Romero, T.-Y. Lin, and M.-Y. Liu. 2024. Meshtron: High-Fidelity, Artist-Like 3D Mesh Generation at Scale. *arXiv:2412.09548* (2024).
- J. Ho, A. Jain, and P. Abbeel. 2020. Denoising diffusion probabilistic models. *Advances in neural information processing systems* 33 (2020), 6840–6851.
- J. Ho, T. Salimans, A. Gritsenko, W. Chan, M. Norouzi, and D. J. Fleet. 2022. Video diffusion models. *Advances in Neural Information Processing Systems* 35 (2022), 8633–8646.
- D. P. Kingma. 2013. Auto-encoding variational bayes. *arXiv:1312.6114* (2013).
- A. Kokosza, H. Wrede, D. G. Esparza, M. Makowski, D. Liu, D. L. Michels, D. Pirk, and W. Palubicki. 2024. Scintilla: Simulating Combustible Vegetation for Wildfires. *ACM Transaction on Graphics* 43, 4 (7 2024). <https://doi.org/10.1145/3658192>
- J. J. Lee, B. Li, S. Beery, J. Huang, S. Fei, R. A. Yeh, and B. Benes. 2025. Tree-D Fusion: Simulation-Ready Tree Dataset from Single Images with Diffusion Priors. In *European Conference on Computer Vision*. Springer, 439–460.
- J. J. Lee, B. Li, and B. Benes. 2023. Latent L-systems: Transformer-based tree generator. *ACM Transactions on Graphics* 43, 1 (2023), 1–16.
- P. Lewis. 1999. Three-dimensional plant modelling for remote sensing simulation studies using the Botanical Plant Modelling System. *Agronomie* 19, 3–4 (1999), 185–210.
- B. Li, J. Kalužny, J. Klein, D. L. Michels, W. Palubicki, B. Benes, and S. Pirk. 2021. Learning to Reconstruct Botanical Trees from Single Images. *ACM Transaction on Graphics* 40, 6, Article 231 (12 2021). <https://doi.org/10.1145/3478513.3480525>
- B. Li, J. Klein, D. L. Michels, S. Pirk, B. Benes, and W. Palubicki. 2023. Rhizomorph: The Coordinated Function of Shoots and Roots. *ACM Transaction on Graphics* 42, 4 (8 2023). <https://doi.org/10.1145/3592145>
- Y. Li, Z. Liu, B. Benes, X. Zhang, and J. Guo. 2024. SVDTree: Semantic Voxel Diffusion for Single Image Tree Reconstruction. In *Proceedings of the IEEE/CVF Conference on Computer Vision and Pattern Recognition*. 4692–4702.
- A. Lindenmayer. 1968. Mathematical models for cellular interactions in development I. Filaments with one-sided inputs. *Journal of theoretical biology* 18, 3 (1968), 280–299.
- S. Luo and W. Hu. 2021. Diffusion probabilistic models for 3d point cloud generation. In *Proceedings of the IEEE/CVF conference on computer vision and pattern recognition*. 2837–2845.
- F. Maggioli, J. Klein, T. Hädrich, E. Rodolà, W. Palubicki, S. Pirk, and D. L. Michels. 2023. A Physically-inspired Approach to the Simulation of Plant Wilting. In *SIGGRAPH Asia 2023 Conference Papers (SA '23)*. ACM, Article 66, 8 pages.
- M. Makowski, T. Hädrich, J. Scheffczyk, D. Michels, S. Pirk, and W. Palubicki. 2019. Synthetic silviculture: multi-scale modeling of plant ecosystems. *ACM Transactions on Graphics (TOG)* 38, 4 (2019), 1–14.
- M. Na, J. Klein, B. Zhang, W. Palubicki, S. Pirk, and D. L. Michels. 2024. A Lennard-Jones Layer for Distribution Normalization. *Transactions on Machine Learning Research* (2024).
- C. Nash, Y. Ganin, S. A. Eslami, and P. Battaglia. 2020. Polygen: An autoregressive generative model of 3d meshes. In *International conference on machine learning*. PMLR, 7220–7229.
- P. Nawrot, S. Tworowski, M. Tyrolski, L. Kaiser, Y. Wu, C. Szegedy, and H. Michalewski. 2021. Hierarchical transformers are more efficient language models. *arXiv:2110.13711* (2021).
- B. Neubert, T. Franken, and O. Deussen. 2007. Approximate image-based tree-modeling using particle flows. In *ACM SIGGRAPH 2007 papers*. 88–es.
- W. Palubicki, M. Makowski, W. Gajda, T. Hädrich, D. L. Michels, and S. Pirk. 2022. Ecolimates: Climate-response Modeling of Vegetation. *ACM Trans. Graph.* 41, 4, Article 155 (July 2022), 19 pages. <https://doi.org/10.1145/3528223.3530146>
- S. Pirk, M. Jarzabek, T. Hädrich, D. L. Michels, and W. Palubicki. 2017. Interactive Wood Combustion for Botanical Tree Models. *ACM Trans. Graph.* 36, 6, Article 197 (Nov. 2017), 12 pages.
- S. Pirk, T. Niese, T. Hädrich, B. Benes, and O. Deussen. 2014. Windy Trees: Computing Stress Response for Developmental Tree Models. *ACM Trans. Graph.* 33, 6, Article 204 (Nov. 2014).
- P. Prusinkiewicz. 1986. Graphical applications of L-systems. In *Proceedings of graphics interface*, Vol. 86. 247–253.
- P. Prusinkiewicz and A. Lindenmayer. 2012. *The algorithmic beauty of plants*. Springer Science & Business Media.
- W. T. Reeves and R. Blau. 1985. Approximate and probabilistic algorithms for shading and rendering structured particle systems. *ACM siggraph computer graphics* 19, 3 (1985), 313–322.
- H. Shao, T. Kugelstadt, T. Hädrich, W. Palubicki, J. Bender, S. Pirk, and D. L. Michels. 2021. Accurately Solving Rod Dynamics with Graph Learning. In *NeurIPS*.
- Y. Siddiqui, A. Alliegro, A. Artemov, T. Tommasi, D. Sirigatti, V. Rosov, A. Dai, and M. Nießner. 2024. Meshgpt: Generating triangle meshes with decoder-only transformers. In *Proceedings of the IEEE/CVF Conference on Computer Vision and Pattern Recognition*. 19615–19625.
- A. R. Smith. 1984. Plants, fractals, and formal languages. *ACM SIGGRAPH Computer Graphics* 18, 3 (1984), 1–10.
- Y. Song, J. Sohl-Dickstein, D. P. Kingma, A. Kumar, S. Ermon, and B. Poole. 2020. Score-based generative modeling through stochastic differential equations. *arXiv:2011.13456* (2020).
- O. Stava, S. Pirk, J. Kratt, B. Chen, R. Mèch, O. Deussen, and B. Benes. 2014. Inverse procedural modelling of trees. In *Computer Graphics Forum*, Vol. 33. Wiley Online Library, 118–131.
- J. Tang, Z. Li, Z. Hao, X. Liu, G. Zeng, M.-Y. Liu, and Q. Zhang. 2024. Edgerunner: Auto-regressive auto-encoder for artistic mesh generation. *arXiv:2409.18114* (2024).
- A. Vaswani. 2017. Attention is all you need. *Advances in Neural Information Processing Systems* (2017).
- B. Wang, Y. Zhao, and J. Barbič. 2017. Botanical Materials Based on Biomechanics. *ACM Trans. Graph.* 36, 4, Article 135 (jul 2017), 13 pages.
- P.-S. Wang. 2023. OctFormer: Octree-based Transformers for 3D Point Clouds. *ACM Transactions on Graphics (SIGGRAPH)* 42, 4 (2023).
- Z. Wang, J. Lorraine, Y. Wang, H. Su, J. Zhu, S. Fidler, and X. Zeng. 2024. LLaMA-Mesh: Unifying 3D Mesh Generation with Language Models. *arXiv:2411.09595* (2024).
- H. Weng, Y. Wang, T. Zhang, C. Chen, and J. Zhu. 2024. PivotMesh: Generic 3D Mesh Generation via Pivot Vertices Guidance. *arXiv:2405.16890* (2024).
- R. Wightman. 2019. PyTorch Image Models. <https://github.com/rwightman/pytorch-image-models>. <https://doi.org/10.5281/zenodo.4414861>
- X. Wu, L. Jiang, P.-S. Wang, Z. Liu, X. Liu, Y. Qiao, W. Ouyang, T. He, and H. Zhao. 2024. Point Transformer V3: Simpler, Faster, Stronger. In *CVPR*.
- B. Zhang, J. Tang, M. Niessner, and P. Wonka. 2023. 3dshape2vecset: A 3d shape representation for neural fields and generative diffusion models. *ACM Transactions on Graphics (TOG)* 42, 4 (2023), 1–16.
- B. Zhang and P. Wonka. 2024. Lagem: A large geometry model for 3d representation learning and diffusion. *arXiv:2410.01295* (2024).
- Y. Zhao and J. Barbič. 2013. Interactive Authoring of Simulation-Ready Plants. *ACM Trans. Graph.* 32, 4, Article 84 (jul 2013), 12 pages.
- X. Zhou, B. Li, B. Benes, S. Fei, and S. Pirk. 2023. Deeptree: Modeling trees with situated latents. *arXiv:2305.05153* (2023).



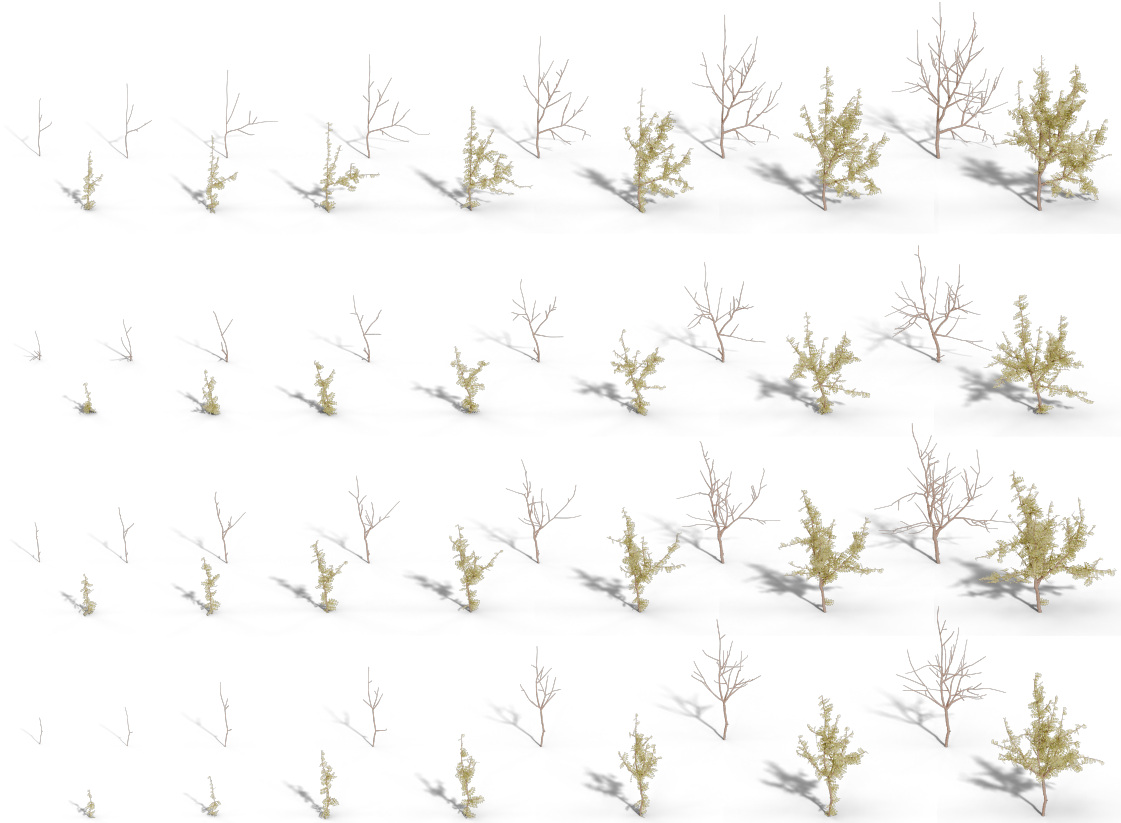
Autoregressive Generation of Static and Growing Trees



Figure 11: Unconditional generation of different tree species.



**Figure 12: An illustration of tree completion. We show the input (left) and multiple different completions (right).**



**Figure 13: Unconditional generation of growing trees.**